

Ionization Energy of Liquid Water Revisited

Conaill F. Perry, Pengju Zhang, Fernanda B. Nunes, Inga Jordan, Aaron von Conta, and Hans Jakob Wörner*



Cite This: *J. Phys. Chem. Lett.* 2020, 11, 1789–1794



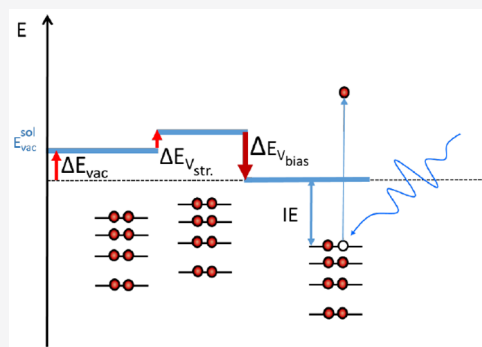
Read Online

ACCESS |

Metrics & More

Article Recommendations

ABSTRACT: The ionization energy of liquid water is one of its most fundamental properties, an important benchmark for first-principles electronic-structure calculations and a crucial reference in the growing field of liquid-phase photoelectron spectroscopy. Despite this significance, a consensus on its value appears to be missing in the literature. Therefore, we use a monochromatized high-harmonic light source to perform detailed measurements of the ionization energy of liquid water in the presence of a tunable bias voltage applied to the liquid jet. Our results suggest that this simple method is sufficient to simultaneously compensate the effects of the streaming potential and that of the vacuum-level offset between the liquid and the photoelectron spectrometer. Our measurements yield corrected values of the vertical and adiabatic ionization energies of the $1b_1$ band of bulk liquid water of 11.67(15) and 10.12(15) eV, respectively. Our method is broadly applicable and is likely to result in corrections to the measured ionization energies of solvated species as well.



The ionization energy (IE) is the most fundamental property determined by photoelectron spectroscopy. IEs of gases and solids have been extensively documented since the discovery of the photoelectric effect.¹ However, gaining access to this information in liquids has been hampered by experimental complications such as studying equilibrated liquids in a high vacuum. Liquid microjets, which allay these experimental difficulties, have become a well-established technique over the last 20 years within the photoelectron community.^{2–20} It is well known that the study of molecules, salts, and other soluble media within an aqueous environment is paramount to developing an understanding of these particles in their natural environment. Therefore, it is of great importance to develop the techniques surrounding liquid-jet photoelectron spectroscopy to reach a deeper understanding of the electronic structure of water and other solvents. Experimental progress on understanding the basic physical properties of liquid water also lays the groundwork for further advances in the understanding of all types of electronic dynamics in aqueous solutions.

Previous studies^{3,16} using both synchrotron and table-top light sources, as well as theoretical work,^{21,22} have provided insight into the IEs of the core and valence orbitals of liquid water. However, the experimentally determined energies have so far not converged, neither with one another nor with theory. Kinematic charging of the liquid microjet,^{2,16,23,24} which is the origin of the streaming potential (V_{str}), is one such cause of the discrepancy between results. Kurahashi et al.¹⁶ observed kinetic energy shifts of the electrons escaping from the gas phase

surrounding the liquid jet, which depended on the distance from the point of ionization to the jet. By tuning the concentration of salt dissolved in the aqueous solution, they were able to reduce the contribution from V_{str} to the limit of neutralizing the effect.

More recent work by Tissot et al.²⁵ showed through photoemission measurements of saturated salt solutions on a gold surface that the respective Fermi levels were equilibrated. In a followup study performed with liquid microjets, Olivieri et al.²⁶ observed consistent effects. They concluded that the different work functions of the aqueous solution and the photoelectron analyzer resulted in an energetic offset between the respective vacuum levels that depended on the composition of the spectrometer and that of the studied solution, hence providing one possible reason for the discrepancies between ionization energies reported by different research groups.

In this work, we propose a straightforward experimental technique for simultaneously compensating for the effects of the streaming potential and the vacuum-level offset. The application of this technique leads us to propose a corrected value for the IE of liquid water.

Received: November 17, 2019

Accepted: January 24, 2020

Published: January 24, 2020

Figure 1 depicts a schematic representation of both of the aforementioned effects relating to a shift in the photoelectron

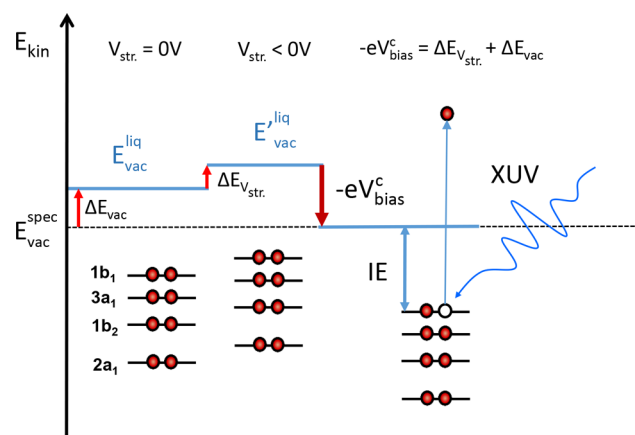


Figure 1. Schematic depicting the effects of the vacuum-level offset and the kinematic charging of the liquid microjet on the binding energies of liquid water. The dashed line indicates the vacuum level of the photoelectron spectrometer.

kinetic energies (PKEs) originating from the valence orbitals (or bands) of $\text{H}_2\text{O}_{(l)}$. On the left, assuming $V_{\text{str}} = 0 \text{ V}$, we illustrate the effect of the vacuum-level offset, which is defined by $E_{\text{vac}}^{\text{liq}} - E_{\text{vac}}^{\text{spec}} = \Delta E_{\text{vac}}$. Because of the metallic composition of the spectrometer, its work function is usually lower than that of water, and hence the vacuum level of the solution lies above that of the spectrometer whenever the respective Fermi levels are equilibrated.²⁵ The central part depicts the additional shift that results from the kinematic charging of the jet. Depending on the nature and concentration of salt in the aqueous solution as well as other experimental parameters, V_{str} can be either positive or negative. Here, for clarity, we only show the effect of a negative potential. The key idea in our work is that the application of an external bias potential, V_{bias}^c , can compensate for both effects simultaneously, effectively equilibrating the vacuum levels of the liquid and the spectrometer and compensating the streaming potential at the same time, as shown in the right-hand part of Figure 1. It is under this condition that we measure the IE.

Tunable extreme ultraviolet (XUV) radiation used in this study is provided by a time-preserving monochromator described in a previous publication.²⁷ High-harmonic generation is driven by laser pulses of 1 mJ energy and 28 fs pulse duration centered at 800 nm with a repetition rate of 5 kHz. The pulses are focused into a semi-infinite gas cell filled with 20 mbar argon. The generated high harmonics are then recollimated by a toroidal mirror, energy-dispersed by a plane grating in a conical-diffraction geometry, and refocused with a second toroidal mirror onto a 200 μm slit. The slit is then imaged with a third toroidal mirror into the interaction region of a 1 m long magnetic-bottle photoelectron spectrometer.²⁸ The spectrometer resolution is 0.14 to 0.34 eV over the investigated kinetic energy range.²⁹ A double-nozzle setup allows for the calibration of photon energies over a typical range of 15–40 eV in gaseous argon and the subsequent measurement of liquid water using a quartz 25 μm inner-diameter liquid jet nozzle. The calibration of the photoelectron spectrometer with argon is repeated every time a new liquid-phase measurement is performed. The nozzle holder and mounting system are both made of PEEK and graphite-coated

to ensure electrical conductivity. The nozzle is capped by Cu tape, covered by a layer of Sn solder, to prevent the insulating quartz from charging up due to stray electrons. All exposed external components are set to ground. (See Figure 2.) All

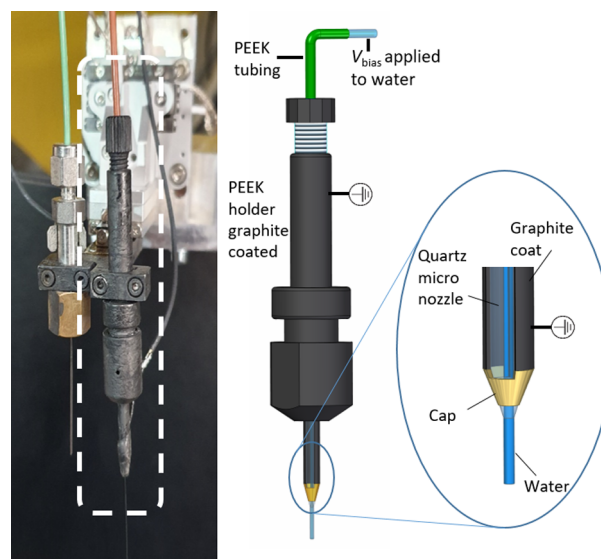


Figure 2. Photograph of liquid-jet nozzle holder alongside a schematic representation. It should be noted that the V_{bias} is applied to the solution outside the chamber.

measurements reported in this publication are performed on a 50 mM aqueous solution of NaCl in high-purity water (Milli-Q) with a measured electrical resistivity of 18.2 $\text{M}\Omega\cdot\text{cm}$, unless stated otherwise. All data are recorded with a flow rate of 0.35 mL/min, except for the additional data points shown in Figure 4b. The total electron count rates are kept below 20 counts per laser shot. We have verified that the observed liquid- and gas-phase spectra do not change for count rates ranging from 1 to 50 counts per shot. The XUV focus within these measurements is $\sim 150 \mu\text{m}$ for the initial liquid measurements and $\sim 180 \mu\text{m}$ for the gas-phase displacement measurements discussed in Figure 4.

The determination of the IE of liquid water, while conceptually simple, has a few inherent difficulties associated with it. One aspect is the contribution of the gas-phase spectrum superimposed on the liquid-phase spectrum. The use of liquid microjets allows one to reach high vacuum, but one cannot suppress the evaporation of water from the surface of the jet. Because of the jet's exposed surface typically being smaller than the focus of the ionizing beam, the ionization of gas-phase water and its contribution to the measured photoelectron spectrum cannot be prevented. The gas-phase IEs are, however, extremely well known^{3,30,31} and therefore serve as an independent benchmark to validate our results.

Figure 3a shows a gas-phase water photoelectron spectrum measured at 23.17(7) eV photon energy. This spectrum has been recorded by moving the liquid jet slightly out of the focus. Figure 3b shows the total photoelectron spectrum recorded when the liquid jet is located in the focus of the XUV beam. This spectrum is decomposed into the contributions of gas- and liquid-phase water on the basis of a principal component fit. The method and fit parameters will be described in detail elsewhere.

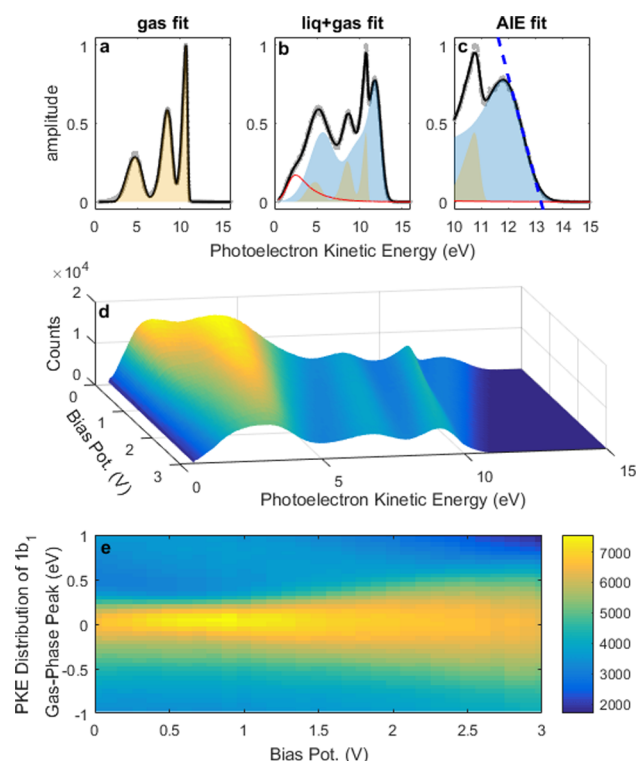


Figure 3. (a) Principal component analysis of the gaseous H_2O spectrum. (b) Principal component analysis of a gas + liquid-phase H_2O spectrum. The gray spectra show the experimental data taken at $h\nu = 23.17(7)$ eV, the black curve indicates the fit, and the yellow and blue shaded regions indicate the gas- and liquid-phase contributions, respectively. The red curve indicates the fitted background dominated by secondary electrons. (c) Determination of the adiabatic ionization energy of the $1b_1$ band. The linear fit is shown by the blue dashed line. (d) Gas + liquid photoelectron spectrum as a function of the applied bias potential. (e) Photoelectron kinetic energy distribution of the gas-phase $1b_1$ band as a function of the applied bias potential.

Figure 3d shows the PKE of the measured liquid-phase spectrum as a function of an applied bias potential. What we observe is that the peaks corresponding to the $1b_{1(g)}$ and $1b_{1(l)}$ bands have a different response to the applied voltage.

Figure 3e shows the PKE distribution of the $1b_{1(g)}$ as a function of the applied bias potential. The scanning of the applied bias potential reveals a narrowing and intensifying of the peak in the range of $V_{\text{bias}} \approx 0$ to 1.0 V. This can be readily explained as a consequence of the potential energy of a photoelectron generated in the vicinity of the liquid jet. This potential energy can be expressed in terms of the electrostatic potential created by the cylindrical jet, which decays logarithmically as a function of distance from the jet. Therefore, any electron born in the vicinity of the jet through the ionization of the surrounding gas phase experiences a different electric-field strength depending on its distance from the jet, leading to a broad kinetic-energy distribution upon reaching the detector. By applying a bias potential and scanning a range of voltages, one can identify a bias potential V_{bias}^c such that $-eV_{\text{bias}}^c = \Delta E_{\text{vac}} + \Delta E_{V_{\text{jet}}}$, where the symbols have been defined in Figure 1. This condition results in a PKE distribution of the electrons originating from the gas phase that no longer depends on their birth position relative to the jet.

The actual determination of V_{bias}^c in each data set contributing to our results was done as follows. Fitting

Gaussians to the PKE distribution of the $1b_{1(g)}$ band and extracting the full width at half-maximum proved unreliable due to the spectral overlap between the gas-phase and liquid-phase signals. Therefore, to determine the narrowest PKE distribution from the $1b_{1(g)}$ band, we extracted the gradient of the rising edge with respect to photoelectron kinetic energy because the narrowest and most intense distribution will have the steepest gradient. Our measurements show the narrowest gas-phase distribution at a bias potential of typically 0.6 V, which is much larger than the streaming potential offset alone at these concentrations according to ref 16. The determination of the $1b_{1(g)}$ IE at the precise bias potential determined from each of our data sets reveals a reproducible peak position of 12.65(9) eV, which agrees very well with the literature value.^{30,31}

We note that simply subtracting a gas-phase spectrum from the acquired gas + liquid spectrum may not yield the correct liquid-phase photoelectron spectrum because the presence of any potential difference, whether experimentally applied or originating from the inherent streaming potential or vacuum-level offset, induces a different kinetic energy response from the gas- and liquid-phase components.

To confirm our application of a bias potential as a valid method for the determination of ionization energies, we performed two additional measurements inspired by the work of Kurahashi et al.,¹⁶ the results of which are shown in Figure 4. By scanning the distance of the jet from the XUV focus position, one can observe the effect of the presence of the liquid jet on the kinetic energy of the gas-phase electrons. (See Figure 4a.) The red curve indicates the data taken without a bias potential applied; the blue curve shows data with a bias of +0.60 V applied. The chosen step size of 200 μm , being larger

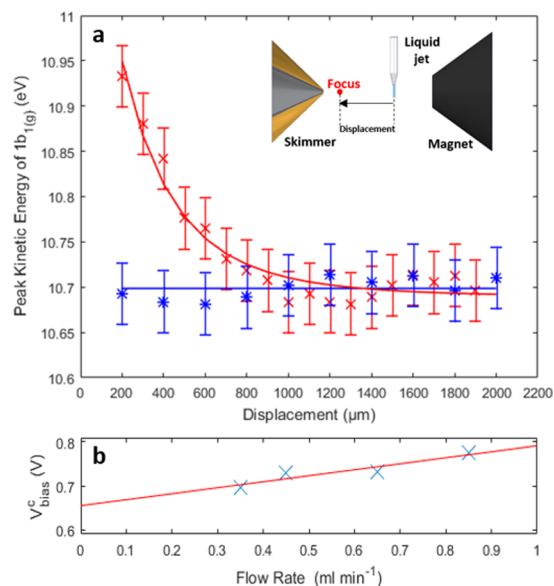


Figure 4. (a) Measured ionization energy of $1b_{1(g)}$ as a function of the distance of the jet from the XUV focus position. The red curve indicates data points without a bias potential. The blue curve indicates data points with a bias of +0.60 V applied. The inset outlines the geometry of the interaction chamber for this measurement. These data points were recorded with a photon energy $h\nu = 23.34(9)$ eV. (b) Flow-rate dependence of V_{bias}^c required to minimize the width of the $1b_{1(g)}$ peak. The red curve indicates the linear fit, including its extrapolation to the zero flow rate.

than the XUV spot size, ensured that we did not observe any liquid-phase contribution in these measurements. Within the limits of our measurement, the peak position for the compensated potential case is essentially flat, indicating that the potential landscape experienced by the photoelectrons within the interaction chamber is equivalent at all points in space. This also indicates that even at a distance of 0.5 mm from the jet, the residual electrostatic potential originating from the running liquid jet cannot be ignored. However, as can be seen, at larger displacements, one reaches the asymptotic limit of this residual electrostatic potential, indicating that our calibration procedure of the photon energy and time-of-flight parameters using argon as a reference and performed at ~ 16 mm from the liquid jet is not affected by the presence of the liquid microjet.

It is known that the kinematic charging of the liquid jet and hence the observed streaming potential are not only salt-concentration-dependent¹⁶ but also dependent on the flow rate of the jet.³² In Figure 4b, we show the values of V_{bias}^c determined at different flow rates. Because the streaming potential is linearly proportional to the flow rate in the first approximation,²³ we use a linear extrapolation of the data to the point of zero flow. The fact that the linear extrapolation of V_{bias}^c to zero flow rate yields a finite value indicates the dominant contribution of the vacuum-level offset to the required bias potential. However, one cannot practically realize the zero-flow-rate situation with a liquid microjet. Therefore, our best estimate for the vacuum-level offset under the experimental conditions of the data shown in Figure 4b is 0.65(5) eV. We note that the exact values of V_{bias}^c change from day to day, which we attribute to small changes of the vacuum-level offset and streaming potential.

Averaging over 83 gas-phase measurements, we obtain a gas phase IE of 12.65(9) eV when the compensation bias is identified and applied. This IE includes measurements conducted using harmonic orders ranging from 15 to 21, corresponding to photon energies of 21.17(7)–32.45(9) eV. This value for the IE is in excellent agreement with the literature data.^{30,33} It is important to emphasize that the IE of $1b_{1(g)}$ has not been used to calibrate the PKE axis but has been determined independently. The agreement with the established literature value validates the principle of our method.

As an additional measure of the robustness of the methodology described herein, experiments were also performed on different salt solutions at concentrations of 10, 30, 100, and 500 mM NaCl in aqueous solution. The same procedure as described above was followed, and a qualitatively similar behavior was observed with respect to both the displacement of the jet from the focus measurement described in Figure 4 and the band-narrowing analysis of the $1b_{1(g)}$. The measurements on the four solutions yielded a gas-phase IE at 12.65(6) eV when compensated by the individually determined bias potentials.

Using the gas phase as an indication that extraneous sources of kinetic energy shifts have been compensated for, we observe a vertical IE for the $1b_{1(l)}$, defined as the maximum of the corresponding liquid-phase photoelectron band of 11.67(15) eV. This IE is higher than previously reported vertical IEs of the $1b_{1(l)}$ (11.16(4)³ and 11.31(4) eV¹⁶). Our determined liquid-phase IE represents data averaged from 63 measurements and accumulated using the same photon energies as the gas-phase measurements (21.17(7)–32.45(9) eV). On the basis of these results, we also determine a $1b_{1(l)}$ and $1b_{1(g)}$

binding-energy difference of 0.99(9) eV, which might be a useful measure for future experiments when absolute IEs are not easily accessible.

By linearly extrapolating from the inflection point of the $1b_{1(l)}$ peak to the baseline (see Figure 3c), we determine an adiabatic IE of 10.12(15) eV. This value is higher than the 9.9 eV of Winter et al.³ but agrees within the error bar with the 10.06 eV value of Delahay et al.,³⁴ although the latter was determined with a different method and might not be directly comparable.


We note that our result agrees well with the most recent theoretical work, which predicts an adiabatic IE of 10.25 eV (“quantum bulk” value) by combining path-integral molecular dynamics with ab initio potentials and many-body perturbation theory.²² We note, however, that our value of the adiabatic IE is susceptible to the exact shape of the measured photoelectron spectrum, which makes it slightly less reliable than our vertical IE as a consequence of the extrapolation procedure illustrated in Figure 3c.

Previous work³⁵ reported both adiabatic and vertical ionization energies using first-principles molecular dynamics and density functional theory. The highest levels of theory based on the so-called range-separated hybrid (RSH) and self-consistent hybrid (sc-hybrid) functionals predicted values of 10.66 or 11.15 eV for the vertical IE and 9.57 or 10.08 eV for the adiabatic IE. These values for the adiabatic IEs are consistently lower than the corresponding latest theoretical results,²² suggesting that further improvements in theory might also converge to a higher vertical IE.

In conclusion, we have demonstrated a straightforward experimental technique that allows for the compensation of adverse electric fields and their effects on binding energies measured by liquid-phase photoelectron spectroscopy. By using the width of the gas-phase photoelectron peak as an in situ sensor of the inhomogeneity of the electrostatic potential distribution, we identified a reliable observable for the determination of the correct compensation voltage to be applied to the liquid jet. Under these conditions, we determined values of 11.67(15) and 10.12(15) eV for the vertical and adiabatic ionization energies of liquid water, respectively. Under the same experimental conditions, we simultaneously obtained a vertical IE of 12.65(9) eV for the $1b_{1(g)}$, which we consider to validate our conclusions.

AUTHOR INFORMATION

Corresponding Author

Hans Jakob Wörner – *Laboratorium für Physikalische Chemie, ETH Zurich 8093 Zurich, Switzerland*;  orcid.org/0000-0002-8877-0872; Email: hwoerner@ethz.ch

Authors

Conaill F. Perry – *Laboratorium für Physikalische Chemie, ETH Zurich 8093 Zurich, Switzerland*

Pengju Zhang – *Laboratorium für Physikalische Chemie, ETH Zurich 8093 Zurich, Switzerland*

Fernanda B. Nunes – *Laboratorium für Physikalische Chemie, ETH Zurich 8093 Zurich, Switzerland*

Inga Jordan – *Laboratorium für Physikalische Chemie, ETH Zurich 8093 Zurich, Switzerland*

Aaron von Conta – *Laboratorium für Physikalische Chemie, ETH Zurich 8093 Zurich, Switzerland*

Complete contact information is available at:
<https://pubs.acs.org/10.1021/acs.jpcllett.9b03391>

Notes

The authors declare no competing financial interest.

ACKNOWLEDGMENTS

We thank Stephan Thürmer, Matthew Brown, Toshinori Suzuki, Bernd Winter and Thomas Allison for helpful discussions. We acknowledge the essential contributions of Andreas Schneider and Mario Seiler to the electronic and mechanical components used in our work. This research was funded by ETH Zurich, the Swiss National Science Foundation through the NCCR-MUST and project 20021_172846, as well as an ERC Consolidator Grant (772797-ATTOLIQ).

REFERENCES

- (1) Einstein, A. Über einen die Erzeugung und Verwandlung des Lichtes betreffenden heuristischen Gesichtspunkt. *Ann. Phys.* **1905**, *322*, 132–148.
- (2) Faubel, M.; Steiner, B.; Toennies, J. P. Photoelectron spectroscopy of liquid water, some alcohols, and pure nonane in free micro jets. *J. Chem. Phys.* **1997**, *106*, 9013–9031.
- (3) Winter, B.; Weber, R.; Widdra, W.; Dittmar, M.; Faubel, M.; Hertel, I. V. Full Valence Band Photoemission from Liquid Water Using EUV Synchrotron Radiation. *J. Phys. Chem. A* **2004**, *108*, 2625–2632.
- (4) Garrett, B. C.; Dixon, D. A.; Camaioni, D. M.; Chipman, D. M.; Johnson, M. A.; Jonah, C. D.; Kimmel, G. A.; Miller, J. H.; Rescigno, T. N.; Rossky, P. J.; et al. Role of Water in Electron-Initiated Processes and Radical Chemistry: Issues and Scientific Advances. *Chem. Rev.* **2005**, *105*, 355–390.
- (5) Winter, B.; Weber, R.; Hertel, I. V.; Faubel, M.; Jungwirth, P.; Brown, E. C.; Bradforth, S. E. Electron binding energies of aqueous alkali and halide ions: EUV photoelectron spectroscopy of liquid solutions and combined ab-initio and molecular dynamics calculations. *J. Am. Chem. Soc.* **2005**, *127*, 7203–7214.
- (6) Winter, B.; Faubel, M. Photoemission from liquid aqueous solutions. *Chem. Rev.* **2006**, *106*, 1176–1211.
- (7) Winter, B.; Aziz, E. F.; Hergenbahn, U.; Faubel, M.; Hertel, I. V. Hydrogen bonds in liquid water studied by photoelectron spectroscopy. *J. Chem. Phys.* **2007**, *126*, 124504.
- (8) Winter, B.; Hergenbahn, U.; Faubel, M.; Björneholm, O.; Hertel, I. V. Hydrogen bonding in liquid water probed by resonant Auger-electron spectroscopy. *J. Chem. Phys.* **2007**, *127*, 094501.
- (9) Aziz, E. F.; Ottosson, N.; Faubel, M.; Hertel, I. V.; Winter, B. Interaction between liquid water and hydroxide revealed by core-hole de-excitation. *Nature* **2008**, *455*, 89–91.
- (10) Jungwirth, P.; Winter, B. Ions at Aqueous Interfaces: From Water Surface to Hydrated Proteins. *Annu. Rev. Phys. Chem.* **2008**, *59*, 343–366.
- (11) Brown, M. A.; Faubel, M.; Winter, B. X-Ray photo- and resonant Auger-electron spectroscopy studies of liquid water and aqueous solutions. *Annu. Rep. Prog. Chem., Sect. C: Phys. Chem.* **2009**, *105*, 174–212.
- (12) Ottosson, N.; Faubel, M.; Bradforth, S. E.; Jungwirth, P.; Winter, B. Photoelectron spectroscopy of liquid water and aqueous solution: Electron effective attenuation lengths and emission-angle anisotropy. *J. Electron Spectrosc. Relat. Phenom.* **2010**, *177*, 60–70.
- (13) Tang, Y.; Suzuki, Y. I.; Shen, H.; Sekiguchi, K.; Kurahashi, N.; Nishizawa, K.; Zuo, P.; Suzuki, T. Time-resolved photoelectron spectroscopy of bulk liquids at ultra-low kinetic energy. *Chem. Phys. Lett.* **2010**, *494*, 111–116.
- (14) Horio, T.; Shen, H.; Adachi, S.; Suzuki, T. Photoelectron spectra of solvated electrons in bulk water, methanol, and ethanol. *Chem. Phys. Lett.* **2012**, *535*, 12–16.
- (15) Thürmer, S.; Seidel, R.; Faubel, M.; Eberhardt, W.; Hemminger, J. C.; Bradforth, S. E.; Winter, B. Photoelectron angular distributions from liquid water: Effects of electron scattering. *Phys. Rev. Lett.* **2013**, *111*, 1–5.
- (16) Kurahashi, N.; Karashima, S.; Tang, Y.; Horio, T.; Abulimiti, B.; Suzuki, Y. I.; Ogi, Y.; Oura, M.; Suzuki, T. Photoelectron spectroscopy of aqueous solutions: Streaming potentials of NaX (X = Cl, Br, and I) solutions and electron binding energies of liquid water and X⁻. *J. Chem. Phys.* **2014**, *140*, 174506.
- (17) Seidel, R.; Winter, B.; Bradforth, S. E. Valence Electronic Structure of Aqueous Solutions: Insights from Photoelectron Spectroscopy. *Annu. Rev. Phys. Chem.* **2016**, *67*, 283–305.
- (18) Kumar, G.; Roy, A.; McMullen, R. S.; Kutagulla, S.; Bradforth, S. E. The influence of aqueous solvent on the electronic structure and non-adiabatic dynamics of indole explored by liquid-jet photoelectron spectroscopy. *Faraday Discuss.* **2018**, *212*, 359–381.
- (19) Pohl, M. N.; Muchová, E.; Seidel, R.; Ali, H.; Sršen, Š.; Wilkinson, L.; Winter, B.; Slavíček, P. Do water's electrons care about electrolytes? *Chemical Science* **2019**, *10*, 848.
- (20) Buttersack, T.; Mason, P. E.; McMullen, R. S.; Martinek, T.; Brezina, K.; Hein, D.; Ali, H.; Kolbeck, C.; Schewe, C.; Malerz, S.; et al. Valence and Core-Level X-ray Photoelectron Spectroscopy of a Liquid Ammonia Microjet. *J. Am. Chem. Soc.* **2019**, *141*, 1838–1841.
- (21) Nordlund, D.; Odelius, M.; Bluhm, H.; Ogasawara, H.; Pettersson, L. G.; Nilsson, A. Electronic structure effects in liquid water studied by photoelectron spectroscopy and density functional theory. *Chem. Phys. Lett.* **2008**, *460*, 86–92.
- (22) Gaiduk, A. P.; Pham, T. A.; Govoni, M.; Paesani, F.; Galli, G. Electron affinity of liquid water. *Nat. Commun.* **2018**, *9*, 247.
- (23) Preissler, N.; Buchner, F.; Schultz, T.; Lübcke, A. Electrokinetic charging and evidence for charge evaporation in liquid microjets of aqueous salt solution. *J. Phys. Chem. B* **2013**, *117*, 2422–2428.
- (24) Brown, M. A.; Abbas, Z.; Kleibert, A.; Green, R. G.; Goel, A.; May, S.; Squires, T. M. Determination of surface potential and electrical double-layer structure at the aqueous electrolyte-nanoparticle interface. *Phys. Rev. X* **2016**, *6*, 1–12.
- (25) Tissot, H.; Gallet, J. J.; Bourmel, F.; Olivieri, G.; Silly, M. G.; Sirotti, F.; Boucly, A.; Rochet, F. The Electronic Structure of Saturated NaCl and NaI Solutions in Contact with a Gold Substrate. *Top. Catal.* **2016**, *59*, 605–620.
- (26) Olivieri, G.; Goel, A.; Kleibert, A.; Cvetko, D.; Brown, M. A. Quantitative ionization energies and work functions of aqueous solutions. *Phys. Chem. Chem. Phys.* **2016**, *18*, 29506–29515.
- (27) Von Conta, A.; Huppert, M.; Wörner, H. J. A table-top monochromator for tunable femtosecond XUV pulses generated in a semi-infinite gas cell: Experiment and simulations. *Rev. Sci. Instrum.* **2016**, *87*, 073102.
- (28) Jordan, I.; Jain, A.; Gaumnitz, T.; Ma, J.; Wörner, H. J. Photoelectron spectrometer for liquid and gas-phase attosecond spectroscopy with field-free and magnetic bottle operation modes. *Rev. Sci. Instrum.* **2018**, *89*, 053103.
- (29) Jordan, I.; Huppert, M.; Brown, M. A.; Van Bokhoven, J. A.; Wörner, H. J. Photoelectron spectrometer for attosecond spectroscopy of liquids and gases. *Rev. Sci. Instrum.* **2015**, *86*, 123905.
- (30) Kimura, K. *Handbook of HeI Photoelectron Spectra of Fundamental Organic Molecules: Ionization Energies, Ab Initio Assignments, and Valence Electronic Structure for 200 Molecules*; Halsted Press: New York, 1981.
- (31) Banna, M. S.; McQuaide, B. H.; Malutzki, R.; Schmidt, V. The photoelectron spectrum of water in the 30–140 eV photon energy range. *J. Chem. Phys.* **1986**, *84*, 4739–4744.
- (32) Mohiuddin Mala, G.; Li, D.; Werner, C.; Jacobasch, H.-J.; Ning, Y. Flow characteristics of water through a microchannel between two parallel plates with electrokinetic effects. *Int. J. Heat Fluid Flow* **1997**, *18*, 489–496.
- (33) Reutt, J. E.; Wang, L. S.; Lee, Y. T.; Shirley, D. A. Molecular beam photoelectron spectroscopy and femtosecond intramolecular dynamics of H₂O⁺ and D₂O⁺. *J. Chem. Phys.* **1986**, *85*, 6928–6939.
- (34) Delahay, P.; Von Burg, K. Photoelectron emission spectroscopy of liquid water. *Chem. Phys. Lett.* **1981**, *83*, 250–254.

(35) Pham, T. A.; Govoni, M.; Seidel, R.; Bradforth, S. E.; Schwegler, E.; Galli, G. Electronic structure of aqueous solutions: Bridging the gap between theory and experiments. *Science advances* 2017, 3, No. e1603210.